HIGH-ORDER NONLINEARLY STABLE ARTIFICIAL DISSIPATION SPECTRAL COLLOCATION OPERATORS FOR THE 1-D UNSTEADY NAVIER-STOKES EQUATIONS

Johnathon Upperman & Nail Yamaleev
Old Dominion University

Abstract

High-order numerical methods that satisfy a discrete analog of the entropy inequality are uncommon. We present a new class of high-order entropy stable artificial dissipation (AD) spectral collocation operators for the 1D unsteady Navier-Stokes equations. The new artificial dissipation preserves the super convergence properties of the baseline spectral collocation operators, satisfies the summation-by-parts convention and discrete entropy inequality, thus facilitating a nonlinear L_2-stability proof for the symmetric form of the regularized Navier-Stokes equations. Numerical results demonstrate that the proposed method outperforms conventional approaches in terms of accuracy, shock capturing capabilities, and computational cost.

1. Introduction

Despite the trend of improving capability of aerodynamic flow simulations, modern computational fluid dynamics (CFD) methods have not been able to demonstrate the desired accuracy for transonic and supersonic separated turbulent flows with strong shock waves and contact discontinuities[9, 18]. These discouraging results suggest that to accurately predict complex discontinuous turbulent flows, new high-order/high-resolution, nonlinearly stable numerical methods must be devised and used for this class of problems.

Among various high-resolution methods developed for improving accuracy and efficiency of CFD simulations of discontinuous flows, weighted essentially non-oscillatory (WENO) methods are one of the most widely used approaches because of their ability to provide highly accurate numerical solutions that are nearly free of spurious oscillations[15,19]. Note, however, that these methods introduce dissipation based on the smoothness of a discrete solution rather than on the physics of a problem. We have taken an alternative approach which is based on the underlying physics. Specifically, we regularize the compressible Navier-Stokes equations by adding AD in the form of the viscous term proposed by Brenner which satisfies the first and second law of thermodynamics, ensures positivity of thermodynamic variables, and preserves the translational and rotational invariances of the Navier-Stokes equations[6]. Furthermore, the Brenner's dissipation operator is positive semi-definite, symmetrized by the same entropy variables used for the Navier-Stokes equations, and entropy dissipative, thus preserving the L2 stability of the numerical scheme.

2. Governing Equations

We consider the one-dimensional unsteady compressible Navier-Stokes (NS) equations on the domain $[a,b]\times[0,T]$ which are given by

$$\begin{gathered}\boldsymbol{u}_t + \left(\boldsymbol{f}(\boldsymbol{u})\right)_x = \left(\boldsymbol{f}^v_{\boldsymbol{NS}}(\boldsymbol{u})\right)_x \\ B_l\boldsymbol{u}(a,t) = \boldsymbol{g_l}\,,\ \ B_r\boldsymbol{u}(b,t) = \boldsymbol{g_r} \\ \boldsymbol{u}(x,0) = \boldsymbol{u}_0(x)\end{gathered} \tag{1}$$

where $\boldsymbol{u}$, $\boldsymbol{f}$, and $\boldsymbol{f}^v_{\boldsymbol{NS}}$ are the conservative variables, inviscid and viscous (Navier-Stokes) fluxes, respectively. We also consider the compressible Euler equations

obtained from Eq. (1) by removing the viscous flux on the right-hand side. Without loss of generality, we assume that the domain boundaries are fixed and the boundary conditions are imposed so that the vectors $\boldsymbol{g_l}$ and $\boldsymbol{g_r}$ contain boundary data that are stable in the nonlinear sense. In addition to the NS equations, we also consider modified equations suggested by Brenner. These modified equations referred to as the Brenner-Navier-Stokes (BNS) equations are obtained by replacing the Eulerian mass-based velocity $\boldsymbol{v}_m$ with the fluid-based (Lagrangian) volume velocity $\boldsymbol{v}$ associated to the motion of individual particles in Eq. (1) [1,2,3]. While these two velocities are normally considered equivalent for incompressible flows, for compressible fluids Brenner suggests that they are related by

$$\boldsymbol{v} - \boldsymbol{v_m} = K(\log(\rho))_x \tag{2}$$

where ρ is the density and $0 \leq K$ is a constant. The one-dimensional BNS equations on the domain $[a, b]x[0, T]$ are given by

$$\boldsymbol{u}_t + \left(\boldsymbol{f}(\boldsymbol{u})\right)_x = \left(\boldsymbol{f}_{\boldsymbol{B}}^{\boldsymbol{v}}(\boldsymbol{u})\right)_x \tag{3}$$

where, $\boldsymbol{f}_{\boldsymbol{B}}^{\boldsymbol{v}}$ is given by

$$\begin{bmatrix} K\rho_x \\ K\rho_x v + \frac{4}{3}\mu v_x \\ \frac{4}{3}\mu v_x v + \kappa T_x + \rho_x K\left(\frac{P}{\rho} + \frac{1}{2}v^2 + e\right) \end{bmatrix} \tag{4}$$

where e, P, T, ρ, v, and μ are the specific internal energy, pressure, temperature, density, velocity and dynamic viscosity. K is a nonnegative coefficient that we set equal to $\frac{1}{\rho}$ to guarantee that the same set of entropies that symmetrize the Euler equations symmetrize $\boldsymbol{f}_{\boldsymbol{B}}^{\boldsymbol{v}}$. The thermal conductivity is represented by κ.

It is well known that in compressible flows strong continuities may develop in finite time even with continuous initial data. The presence of these discontinuities causes the numerical solution to become oscillatory which can lead to nonphysical phenomenon such as negative density. The BNS equations (3) can be used to overcome these problems[6]. The BNS equations are consistent with the First and Second Laws of thermodynamics, the density for weak solutions is positive off a time-space set of Lebesgue measure zero, and the diffusion effectively damps possible oscillations of the density and other fields. Thus, we propose to regularize the NS equations by adding the viscous term proposed by Brenner

$$\boldsymbol{u}_t + \left(\boldsymbol{f}(\boldsymbol{u})\right)_x = \left(\boldsymbol{f}_{\boldsymbol{NS}}^{\boldsymbol{v}}(\boldsymbol{u})\right)_x + \left(\boldsymbol{\beta}\boldsymbol{f}_{\boldsymbol{B}}^{\boldsymbol{v}}(\boldsymbol{u})\right)_x \tag{5}$$

where $\boldsymbol{f}_{\boldsymbol{B}}^{\boldsymbol{v}}$ is the Brenner viscous flux, $\boldsymbol{\beta}$ is a nonnegative function that controls the amount and location of AD, and $\boldsymbol{f}_{\boldsymbol{NS}}^{\boldsymbol{v}}$ is the original viscous flux from the NS equations.

3. Continuous Entropy Estimate

For problems with shock waves and contact discontinuities, weak solutions of (1) should be considered. It is well known that the weak solutions in general may not be unique[14]. This problem can be overcome by selecting a physically relevant solution that satisfies an entropy condition, which is a statement of the second law of thermodynamics. From a mathematical viewpoint, the entropy can be defined as a convex scalar function, $S(\boldsymbol{u})$, with an entropy flux, $F(\boldsymbol{u})$, defined by the following differential relation[11]:

$$S_{\boldsymbol{u}} f_{\boldsymbol{u}} = F_{\boldsymbol{u}}. \tag{6}$$

Since the entropy function is convex, its Hessian is positive definite if two thermodynamic variables (e.g., density and

temperature) are positive in the entire domain, thus yielding a one-to-one mapping from the conservative to entropy variables,

$$S_{\boldsymbol{u}} = \boldsymbol{w}^T \tag{7}$$

The existence of an entropy function is in general not guaranteed for an arbitrary nonlinear system of equations due to the large number of constraints it must satisfy. For the Euler equations, it has been shown that there is a family of entropy variables that satisfy Eq. (7) and symmetrize the Jacobian of the inviscid flux[12]. Note, however, that there is only one set of entropy variables in this family that makes the diffusive coefficient matrix in Eq. (1) symmetric[21]. These entropy variables and corresponding mathematical entropy are given by

$$\boldsymbol{w} = \left[\frac{h}{T} - s - \frac{v^2}{2T}, \frac{v}{T}, -\frac{1}{T}\right]^T, \qquad S = -\rho s \tag{8}$$

where T, h and v are the temperature, specific enthalpy and velocity, respectively, s is the thermodynamic entropy defined by

$$s = \frac{R}{\gamma - 1}\log\left(\frac{T}{T_0}\right) - R\log\left(\frac{\rho}{\rho_0}\right) \tag{9}$$

and T_0 and ρ_0 are the reference temperature and density, respectively. Expressing the NS equations (1) in terms of these entropy variables yields

$$\begin{aligned} &\boldsymbol{u}_t + \left(\boldsymbol{f}(\boldsymbol{u})\right)_x - \left(\boldsymbol{f}^v(\boldsymbol{u})\right)_x \\ &= \boldsymbol{u}_w \boldsymbol{w}_t + \boldsymbol{f}_w(\boldsymbol{w})\boldsymbol{w}_x - (\mu_{NS}\boldsymbol{w}_x)_x = \boldsymbol{0} \end{aligned} \tag{10}$$

where $\boldsymbol{u}_w = [\boldsymbol{u}_w]^T$, $\boldsymbol{f}_w = [\boldsymbol{f}_w]^T$, and $\mu_{NS} = [\mu_{NS}]^T$ are symmetric matrices. Furthermore, $\boldsymbol{u}_w$ is positive definite if the density and temperature are positive and the viscosity matrix μ_{NS} is positive semi-definite. If the entropy variables symmetrize Eq. (1), the corresponding entropy function S and its flux F satisfy the following equations[11]:

$$\phi = \boldsymbol{w}^T\boldsymbol{u} - S, \qquad \psi = \boldsymbol{w}T\,\boldsymbol{f} - F \tag{11}$$

where the nonlinear functions ϕ and ψ are the entropy potential and the potential flux, respectively. Using the entropy variables that symmetrize Eq. (1), one can show that the convex entropy is bounded from above for the NS equations. Indeed, multiplying Eq. (1) by the entropy variable $\boldsymbol{w}^T\boldsymbol{u} = S_{\boldsymbol{u}}$ yields

$$\begin{aligned} &S_{\boldsymbol{u}}\boldsymbol{u}_t + S_{\boldsymbol{u}}\boldsymbol{f}_{\boldsymbol{u}}\boldsymbol{u}_x = S_t + F_x \\ &= S_{\boldsymbol{u}}\boldsymbol{f}_x^{(v)} = (\boldsymbol{w}^T\boldsymbol{f}^v)_x - \boldsymbol{w}_x^T\mu_{NS}\boldsymbol{w}_x \end{aligned} \tag{12}$$

Integrating Eq. (10) with respect to x, we have

$$\frac{\mathrm{d}}{\mathrm{d}t}\int_a^b S dx = [\boldsymbol{w}^T\boldsymbol{f}^v - F]_a^b - \int_a^b \boldsymbol{w}_x^T\mu_{NS}\boldsymbol{w}_x dx \tag{13}$$

Since the viscosity matrix μ_{NS} is positive semi-definite, the last term in Eq. (13) is negative, thus indicating that the integral of the entropy over the domain can only increase through the boundaries. Equation (13) can be interpreted as the conservation of entropy in the domain—note that the mathematical entropy has the opposite sign from thermodynamic entropy in gas dynamics. It should be emphasized that the equation of conservation of entropy is not valid for discontinuous flows, because it does not account for the dissipation of entropy at shocks and contact discontinuities[13]. Since the entropy dissipates if discontinuities are present in the domain, we have

$$\frac{\mathrm{d}}{\mathrm{d}t}\int_a^b S dx \le [\boldsymbol{w}^T\boldsymbol{f}^v - F]_a^b - \int_a^b \boldsymbol{w}_x^T\mu_{NS}\boldsymbol{w}_x dx. \tag{14}$$

Note that Eq. (14) becomes equality for smooth solutions. The entropy inequality given by Eq. (14) is a necessary condition for selecting a unique, physically relevant solution among the possibly many weak

solutions of Eq. (1). Since the entropy analysis is valid for the Navier-Stokes equations describing under-resolved and discontinuous flows, it is therefore more generally applicable than linear energy analysis and gives a stronger stability estimate.

Since the Brenner's flux is also symmetrized by the same entropy variables used for NS equations, the above continuous analysis applied to (3) gives an inequality analogous to (14)

(15)

$$\frac{\mathrm{d}}{\mathrm{dt}}\int_a^b S dx \le [\boldsymbol{w}^T(\boldsymbol{f}_{\boldsymbol{NS}}^v + \boldsymbol{\beta}\boldsymbol{f}_{\boldsymbol{B}}^v) - F]_a^b - \int_a^b \boldsymbol{w}_{\boldsymbol{x}}^T(\mu_{\boldsymbol{NS}} + \boldsymbol{\beta}\mu_{\boldsymbol{B}})\,\boldsymbol{w}_{\boldsymbol{x}} dx$$

where since $\boldsymbol{\beta}$ is a nonnegative function, and the Brenner's viscosity matrix $\mu_{\boldsymbol{B}}$ is also positive semi-definite we again have that the integral of the entropy over the domain can only increase through the boundaries.

4. Spectral Collocation Method

4.1 High-order diagonal-norm summation-by-parts (SBP) spectral collocation operators

We now turn to constructing discrete spectral collocation operators that mimic the continuous entropy properties at the semi-discrete level.

We discretize the derivatives in Eq. (3) by dividing the interval $[a, b]$ into K non-overlapping elements $[x_l^k, x_r^k]$ with K+1 nonuniformly distributed points, so that $x_l^k = x_r^{k-1}$. Within each element $[x_l^k, x_r^k]$ the local solution is approximated with a polynomial of order p

(16)

$$u_k(x,t) = \sum_{j=1}^{p+1} u_k(x_j^k, t) L_j^k(x) = \boldsymbol{L}(x)^T \boldsymbol{u}_k(\boldsymbol{x}_k, t),$$

where $\boldsymbol{L}(x) = [L_1(x),\ L_2(x),\ \dots, L_{p+1}(x)]^T$ is the vector of Lagrange polynomials and $\boldsymbol{u}_k(x_k,t) = [u_k(x_1^k,t), u_k(x_2^k,t), \dots, u_k(x_{p+1}^k,t)]^T$ is the solution vector associated with *k*-th element. The global solution is approximated by the piecewise pth-order polynomial approximation defined as the direct sum of the *K* local polynomial solutions $u_k(x,t)$. A possible choice for the computational grid inside each element is the Legendre-Gauss-Lobatto (LGL) points. This grid includes the element end points, which allow the operators to be written in terms of flux differences, which facilitates the proof for discrete entropy stability. Since the approximate solution is constructed at local points x_k, they are referred to as solution points. Along with the solution points, we also define a set of intermediate points $\bar{\boldsymbol{x}}_k = [\bar{x}_0^k, \bar{x}_1^k, \dots, \bar{x}_{p+1}^k]^T$ prescribing the bounding control volume about each solution point. Note that $x_1^k = \bar{x}_0^k$ and $\bar{x}_{p+1}^k = x_{p+1}^k$. These points are referred to as flux points. The distribution of flux points depends on the discretization operator and is discussed in the next section. The local semi-discrete weak form of the governing equations (1) or (3) can be discretized by constructing spectral collocation operators that satisfy a discrete analog of the integration-by-parts rule which is hereafter referred to as a summation-by-parts (SBP) condition[5]. This mimetic property is achieved by constructing a local approximation of the first derivative in the following form:

(17)

$$D = P^{-1}Q, \qquad u_x(\boldsymbol{x}) = D\boldsymbol{u} + \mathrm{T}_{p+1},$$

where $u_x(\boldsymbol{x}) = [u_x(x_1), \dots, u_x(x_{p+1})]^T$, T_{p+1} is the (p+1)th-order truncation error, P and Q can be interpreted as local mass and stiffness matrices defined as

(18)

$$P = \sum_j \boldsymbol{L}(x_j)[\boldsymbol{L}(x_j)]^T \sigma_j$$

$$Q = \sum_j \boldsymbol{L}(x_j)[\boldsymbol{L}'(x_j)]^T \sigma_j$$

where x_j are the solution points, i.e., the nodes of the Legendre-Gauss-Lobatto quadrature formula, and σ_j are the corresponding LGL quadrature weights. It can be proven that these local mass and stiffness matrices given by Eq. (18) satisfy the following properties[4]:

(19)

$$P = P^T, \boldsymbol{v}^T P \boldsymbol{v} > 0, \forall \mathbf{v} \neq \mathbf{0}$$
$$Q = B - Q^T, B = diag(-1,0,\dots,0,1)$$

Furthermore, one can show that P is a diagonal matrix[5]. Only diagonal-norm spectral collocation (SC) operators are considered herein, which is critical for obtaining the entropy estimate for the time derivative term in Eq. (1) and (3). Using the definitions of P and Q given by Eq. (18), it can be shown that the derivative operator, D, is pth-order accurate and possesses the following SBP property:

(20)

$$\begin{aligned}\mathbf{v}^T P D \mathbf{u} &= \mathbf{v}^T Q \mathbf{u} = \mathbf{v}^T (B - Q^T) \\ &= v_{\mathrm{p+1}} u_{\mathrm{p+1}} - v_1 u_1 \\ &- (D\mathbf{v})^T P \mathbf{u}.\end{aligned}$$

Thus, D is a SBP operator that mimics the continuous integration-by-parts formula.

4.2 Telescopic flux form

An important element in the current approach is the use of a complementary grid generated by the flux points, $\bar{\mathbf{x}}$. This grid allows the SBP spectral collocation operators to be written as simple flux differences, analogous to those used in finite volume methods. The result is that any high-order spectral collocation scheme can be recast into the telescopic flux form on the complementary grid, which is critical for providing the conservation properties and constructing entropy stable operators[14].

The complementary grid is constructed such that the spacing between the flux points is precisely equal to the diagonal elements of the positive definite matrix P given by Eq. (18), i.e.,

(21)

$$\Delta \bar{\mathbf{x}} = P\mathbf{1},$$

where $\bar{\mathbf{x}} = \left[\overline{x_0}, \dots, \overline{x_{\mathrm{p+1}}}\right]^T$ is the flux point vector, $\mathbf{1} = [1,1,\dots,1]^T$ (dimension p+1), and Δ and $\widetilde{\Delta}$ are $(p+1) \times (p+2)$ matrices corresponding to simple two-point backward difference operators where for $p = 3$ we have

$$\Delta = \begin{bmatrix} -1 & 1 & 0 & 0 & 0 \\ 0 & -1 & 1 & 0 & 0 \\ 0 & 0 & -1 & 1 & 0 \\ 0 & 0 & 0 & -1 & 1 \end{bmatrix};$$
$$\widetilde{\Delta} = \begin{bmatrix} 0 & 1 & 0 & 0 & 0 \\ 0 & -1 & 1 & 0 & 0 \\ 0 & 0 & -1 & 1 & 0 \\ 0 & 0 & 0 & -1 & 0 \end{bmatrix}.$$

All discrete differentiation operators that satisfy the 1-D SBP convention (and their tensor product extensions) given by Eq. (20) can be recast into a telescopic flux form[7],

(22)

$$P^{-1} Q \mathbf{f} = P^{-1} \Delta \bar{\mathbf{f}},$$

where $\bar{\mathbf{f}}$ is a high-order flux vector defined at the flux points. The above telescopic flux form satisfies the following generalized SBP property:

(23)

$$\begin{aligned}v^T P P^{-1} \Delta \bar{\mathbf{f}} &= \overline{f_{\mathrm{p+1}}} v_{\mathrm{p+1}} - \bar{f}_0 v_0 - \sum_{j=0}^{p} \bar{f}_j (v_{j+1} - v_j) \\ &= \overline{f_{\mathrm{p+1}}} v_{\mathrm{p+1}} - \bar{f}_0 v_0 - \bar{\mathbf{f}}^T \widetilde{\Delta} \mathbf{v}.\end{aligned}$$

Note that the above generalized SBP property is instrumental for satisfying the Lax-Wendroff theorem[17].

Like the derivative of the inviscid flux, the discretized viscous operator of the Navier-Stokes equations given by Eq. (1) or that of Brenner equations given by Eq. (3) can also be recast in the telescopic flux form. To mimic the continuous entropy properties, the viscous fluxes must be

written as functions of the discrete gradients of the entropy variables,

$$\left(\hat{\mu} w_x(\mathbf{x})\right)_x \approx P^{-1}\Delta\bar{\mathbf{f}}^{(v)} = P^{-1}(-D^T P[\hat{\mu}]D + B[\hat{\mu}]D)\mathbf{w} \quad \textbf{(24)}$$

where $[\hat{\mu}]$ is the diagonal positive semi-definite viscosity matrix, which is constructed from block-diagonal combinations of positive semi-definite matrices. Note that this discrete viscous operator satisfies a telescoping conservation property, which is identical to that of the inviscid term.

4.3 SSSCE-BSV implementation details

Without the addition of the Brenner flux term, our scheme is identical to the entropy stable spectral collocation element (SSSCE) scheme[5]. We integrate in time using a 4th order five stage low storage[16]. Note that this scheme violates the entropy stability property of the semi-discrete operator by a factor proportional to the local temporal truncation error. Second-order temporal schemes that preserve these properties have been explored[4]. The development of high-order temporal discretization's that retain the entropy stability properties of the spatial operators is an area of ongoing research. At each stage, we begin by calculating the Euler and Navier Stokes fluxes as well as the penalty terms[5]. The spatial derivatives are approximated using the high-order SBP operators presented in Sections 4.1-4.2.

The amount of AD added in each element is controlled by $\boldsymbol{\beta}$ and is done in a manner like the entropy viscosity method[10]. The artificial viscosity coefficient is constructed such that it is proportional to the residual of the entropy equation. Since the residual grows as $O(\Delta x^{-1})$ at strong discontinuities, we bound the entropy viscosity coefficient from above by the quantity that is equivalent to the artificial viscosity of the first-order fully upwind scheme. We also apply the least squares smoothing to $\boldsymbol{\beta}$ to guarantee that the viscosity coefficient is a differentiable function within each element. Once $\boldsymbol{\beta}$ is determined, we add the Brenner artificial dissipation flux contribution to $\frac{d\mathbf{u}}{dt}$ and integrate the discrete solution in time. Given that we are using the Brenner viscous flux and entropy viscosity method to add dissipation to the SSSCE scheme, we refer to this scheme as the SSSCE-BSV scheme.

5. Discrete Entropy Estimate

With the SBP discrete derivative operators in place, the regularized NS equations (3) can be discretized in a single grid element as follows:

$$\frac{d\mathbf{u}}{dt} + P^{-1}\Delta\bar{\mathbf{f}} = P^{-1}\Delta\bar{\boldsymbol{f}}_{NS} + P^{-1}\Delta\boldsymbol{\beta}\bar{\boldsymbol{f}}_B + P^{-1}\mathbf{g}_B, \quad \textbf{(25)}$$

where $\mathbf{g}_B$ is a penalty term, which enforces the interface and boundary conditions. This spectral collocation scheme given by Eq. (25) satisfies a semi-discrete entropy condition that mimics the continuous counterpart, Eq. (15) if some constraints are imposed on the high-order inviscid flux $\bar{\mathbf{f}}$. Indeed, multiplying Eq. (25) by $\mathbf{w}^T P$ from the left, we have

$$\mathbf{w}^T P\frac{d\mathbf{u}}{dt} + \mathbf{w}^T\Delta\bar{\mathbf{f}} = \mathbf{w}^T\Delta\bar{\boldsymbol{f}}_{NS} + \mathbf{w}^T\Delta\boldsymbol{\beta}\bar{\boldsymbol{f}}_B + \mathbf{w}^T\mathbf{g}_B, \quad \textbf{(26)}$$

where $\mathbf{w}^T = \left[w(u_1), \ldots, w(u_{p+1})\right]^T$ is a vector of entropy variables. The semi-discrete entropy estimate is achieved by mimicking, term by term, the continuous estimate outlined above. The estimate has been carried out for the NS equations elsewhere and since the Brenner's flux term can be handled similarly to the NS flux term, we omit the details here[5].

6. Numerical Results

The accuracy and robustness of the schemes developed herein are tested using standard benchmark problems with smooth and discontinuous solutions. The problem with the smooth solution is the propagation of a viscous shock. The problems that have discontinuous solutions include the Lax shock tube problem and the interaction of a shock with an acoustic wave. As a reference, we compare the new artificial dissipation against a conventional residual based dissipation[20].

This scheme is referred to as SSSCE-LFR which is identical to the scheme (25) except for the artificial dissipation term is based on the Laplace operator and the artificial viscosity coefficient is proportional to the residual $L\boldsymbol{u_i} = \mathbf{f_u u_x} - \mathbf{f_x}$. Again, smoothing is applied, so that the artificial dissipation coefficient is linearly interpolated inside the element while its interface value is determined by taking the maximum of two interface residuals.

6.2 Viscous shock

The convection of a viscous shock is used to test the error convergence of our scheme. The exact solution of this test problem can be constructed analytically for the Prandtl number ¾. A full derivation of this exact solution can be found elsewhere[8].

The convergence rate for the viscous shock is evaluated on a sequence of properly nested uniform and nonuniform grids. The shock is initially located in the middle of the domain. The Reynolds number is $Re = 10$ and the reference Mach number is $M = 2.5$. The equations are integrated until $t = 0.2$. The maximum norm of error calculated using the 4th-order SSSCE scheme along with the SSSCE-BSV and SSSCE-LFR methods on the uniform and the nonuniform grids are shown in Figs. 1 & 2. As evident in Figs. 1 & 2, the (p+1)th-order of convergence is achieved on both uniform and nonuniform grids

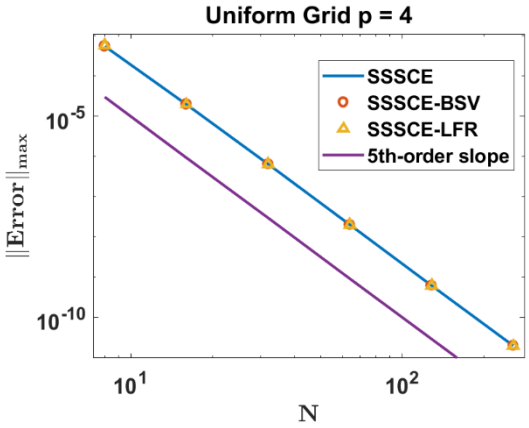

Figure 1 *The max error convergence obtained with 4th-order SSSCE, SSCE-BSV, and SSSCE-LFR schemes on uniform grids for the viscous shock problem.*

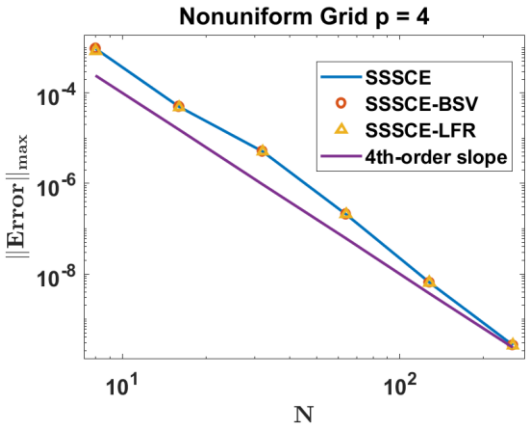

Figure 2 *The max error convergence obtained with 4th-order SSSCE, SSCE-BSV, and SSSCE-LFR schemes on nonuniform grids for the viscous shock problem.*

6.3 Lax shock tube problem

To test the proposed scheme for flows with strong discontinuities, we use the classical Riemann problem of Lax. The initial distributions of the density, velocity, and pressure are

$$(\rho, v, p) = \begin{cases} (0.445, 0.698, 3.528) & \text{for } 0 \le x < 0.5 \\ (0.5, 0, 0.571), & \text{for } 0.5 \le x < 1. \end{cases}$$

We see that while the SSSCE scheme is highly oscillatory for this problem (Fig. 3), the other two methods are quasi-

monotone. Notice that the BSV method is less dissipative at the contact discontinuity and it is slightly more dissipative at the bottom of the shock which prevents it from undershooting (Fig. 4).

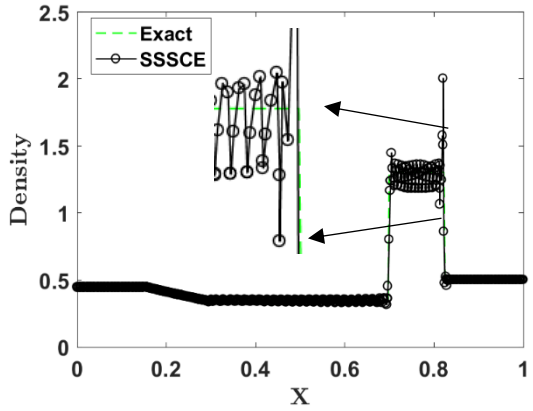

Figure 3 *The comparison of the exact density profile of the Lax problem with the numerical solution of the SSSCE scheme using 4-th order polynomials on each element and 128 elements.*

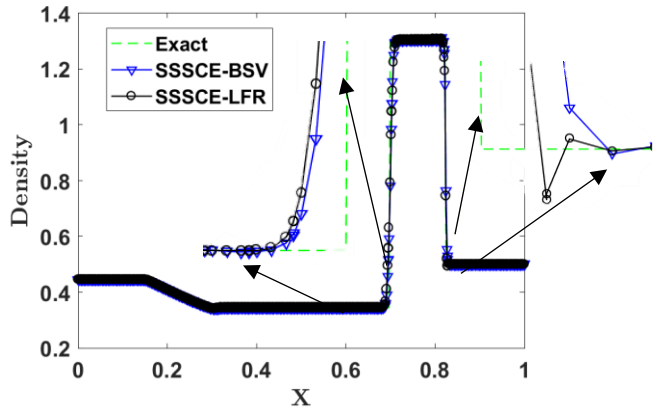

Figure 4 *The comparison of the exact density profile of the Lax problem with the numerical solution of the SSSCE-BSV and SSSCE-LFR scheme using 4-th order polynomials on each element and 128 elements.*

the interaction of a moving shock with smooth density fluctuations. The solution of this benchmark problem contains both strong discontinuities and smooth structures, which is very well suited for testing high-order shock-capturing schemes. The governing equations are the time-dependent 1-D Euler equations subject to the following initial conditions:

$$(\rho, v, p) = \begin{cases} (3.857, 2.629, 10.33), & 0 \le x < 1 \\ (1 + 0.2\sin(5x), 0, 1), & 0.5 \le x < 1 \end{cases}$$

The governing equations are integrated in time up to $t = 1.8$. The exact solution to this problem is not available. Therefore, a numerical solution obtained with the 5th-order Energy Stable WENO finite difference scheme on a uniform grid with 4000 grid cells is used as a reference solution[22].

As expected the SSSCE method is highly oscillatory for this testcase. Also, we see that the LFR method is more dissipative in the smooth regions upstream of the shock but does not dissipate the weak shock sufficiently to avoid an overshoot. In contrast to the LFR scheme the new method is less dissipative in regions where the solution is smooth and provides better shock-capturing capabilities at strong discontinuities.

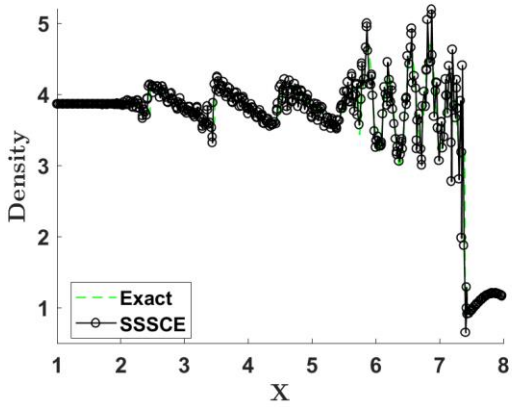

Figure 5 *The comparison of the reference solution of the shock/acoustic wave interaction problem with the numerical results obtained using SSSCE with 4th-order polynomials on each element and 128 elements.*

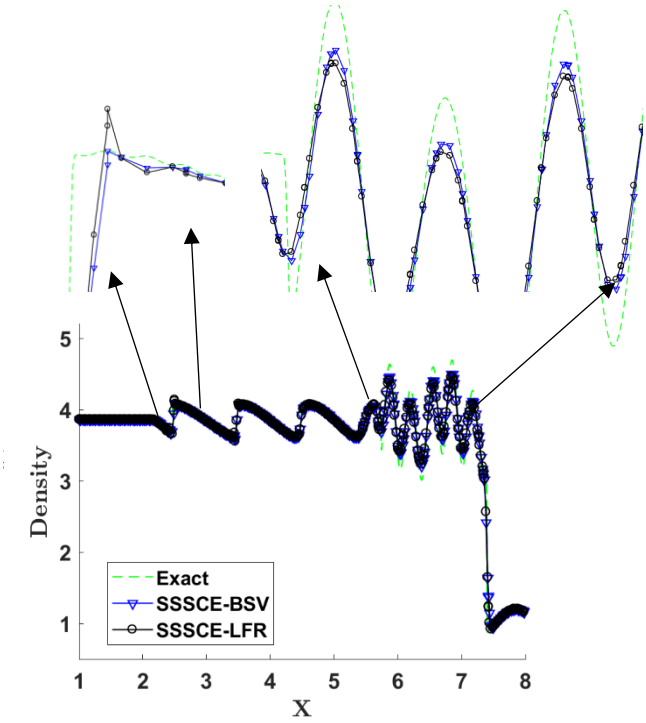

Figure 6 *The comparison of the reference solution of the shock/acoustic wave interaction problem with the numerical results obtained using BSV & LFR with 4th-order polynomials on each element and 128 elements.*

6.5 Computational cost

To determine the computational cost, we used the classical Riemann problem of Sod which includes a rarefaction wave, contact discontinuity and shock. For each polynomial order p and number of elements N, the average time taken to complete one RK time step was recorded for all three methods. Since, the SSSCE -LFR and SSSCE -BSV methods the same underline scheme (SSSCE), the computational costs are calculated relative to the SSSCE cost (i.e. "2" means that for given p, N the CPU time of a given method was on average twice as long per RK time step as compared to the SSSCE method for the same values of p, N). As follows from the results presented in Tables 1 & 2, the computational cost for the LFR method is nearly twice that of the BSV method. While both schemes consistently decrease in computational cost as the polynomial order increases, only the BSV method decreases in computational cost as the number of elements increase—the LFR method has the opposite trend. The decrease in computational cost of the BSV method is due to the inherent switching mechanism which identifies cells that do not need artificial dissipation.

N/p	3	4	5	6
8	3.04	3.02	2.97	2.90
16	3.10	3.08	3.02	2.94
32	3.16	3.14	3.08	3.00
64	3.21	3.20	3.13	3.04
128	3.25	3.21	3.16	3.10

Table 1 *Computational cost for* ***SSSCE-LFR*** *method.*

N/p	3	4	5	6
8	1.70	1.68	1.66	1.62
16	1.67	1.64	1.61	1.58
32	1.65	1.62	1.60	1.58
64	1.64	1.62	1.59	1.55
128	1.64	1.60	1.56	1.54

Table 2 *Computational cost for* ***SSSCE-BSV*** *method.*

7. Conclusion & Future Research

We have presented a new class of high-order entropy stable artificial dissipation (AD) spectral collocation operators for the 1-D unsteady Navier-Stokes equations. The new AD preserves the super convergence properties of the baseline spectral collocation operators, satisfies the summation-by-parts convention and discrete entropy inequality, thus facilitating a nonlinear L_2-stability proof for the symmetric form of the regularized Navier-Stokes equations. When compared to the state-of-the-art artificial dissipation (SSSCE-LFR), we see that the SSSCE-BSV method is less dissipative in smooth regions and contact discontinuities while providing better shock-capturing capabilities at both strong and weak shocks and hence less likely to form nonphysical results such as negative density. Furthermore, the computational cost of the BSV scheme is by a factor of 2 less than that of the conventional counterpart.

The entropy equation residual can also be used as an error estimate to drive a grid adaptation process. Local *r*-refinement (node movement that preserves the grid connectivity) and *h*-refinement (splitting of one grid cell into several cells of smaller size) can be efficiently utilized to minimize the residual of the entropy equation. In addition to constructing new grid adaptation methods, we are also looking into developing fully discrete entropy stable schemes. Currently, we are using an explicit 4th order five stage low storage Runge-Kutta scheme, which does not provide entropy conservation or dissipation. To overcome this problem, we plan to construct new high-order implicit schemes which are entropy stable. One of the advantages of using an implicit scheme is that it is unconditionally stable and does not impose severe bounds on the time step which becomes stricter as the grid is locally refined.

Acknowledgements

J. Upperman was supported by a Virginia Space Grant Consortium Graduate STEM Research Fellowship and a Science, Mathematics And Research for Transformation (SMART) Scholarship. This research was also supported by the Turing High Performance Computing cluster at Old Dominion University.

References

[1] H. Brenner. Fluid mechanics revisited. *Phys. A*, 370:190{224, 2006.

[2] H. Brenner. Kinematics of volume transport. *Phys. A*, 349:11{59, 2005.

[3] H. Brenner. Navier-Stokes revisited. *Phys. A*, 349(1-2):60{132, 2005.

[4] M.H. Carpenter, D. Gottlieb, Spectral methods on arbitrary grids, J. Comput. Phys. 129 (1996) 74–86.

[5] M.H. Carpenter, T.C. Fisher, E.J. Nielsen, S.H. Frankel, Entropy stable spectral collocation schemes for the Navier–Stokes equations: discontinuous inter-faces, SIAM J. Sci. Comput. 36(5) (2014) B835–B867.

[6] E. Feireisl, A. Vasseur, "New perspectives in fluid dynamics: Mathematical analysis of a model proposed by Howard Brenner," Adv. Math. Fluid Mech., Birkhauser-Verlag, Basel, 2010, pp.153-179.

[7] T.C. Fisher, M.H. Carpenter, J. Nordstrom, N.K. Yamaleev, R.C. Swanson, Discretely conservative finite-difference formulations for nonlinear conservation laws in split form: theory and boundary conditions, J. Comput. Phys. 234 (2013) 353–375.

[8] T.C. Fisher, High-Order L2Stable Multi-Domain Finite Difference Method for Compressible Flows, Ph.D. thesis, Purdue University, 2012.

[9] E. Garnier, P. Sagaut, Large eddy simulation of shock/boundary-layer interaction, AIAA J. 40(10) (2002) 1935–1944.

[10] J. Guermond, R. Pasquetti, B. Popov, "Entropy viscosity method for nonlinear conservation laws," Journal of Computational Physics, Vol. 230, 2011, p. 4248-4267.

[11] S.K. Godunov, An interesting class of quasilinear systems, Dokl. Akad. Nauk SSSR 139(3) (1961) 521–523.

[12] A. Harten, On the symmetric form of systems of conservation laws with entropy, J. Comput. Phys. 49 (1983) 151–164.

[13] A. Harten, B. Engquist, S. Osher, S.R. Chakravarthy, Uniformly high order accurate essentially non-oscillatory schemes III, J. Comput. Phys. 71(2) (1987) 231–303.

[14] J. Hesthaven, T. Warburton, Nodal Discontinuous Galerkin Methods: Algorithms, Analysis, and Applications, Texts in Applied Mathematics, Springer, 2008.

[15] G. Jiang, C.-W. Shu, Efficient implementation of weighted ENO schemes, J. Comput. Phys. 126 (1996) 202–228.

[16] C.A. Kennedy, M.H. Carpenter, R.M. Lewis, Low-storage, explicit Runge–Kutta schemes for the compressible Navier–Stokes equations, Appl. Numer. Math. 35(3) (2000) 177–219.

[17] P. Lax, B. Wendroff, Systems of conservation laws, Commun. Pure Appl. Math. 13 (1960) 217–237.

[18] D.W. Levy, et al., Summary of data from the Fifth Computational Fluid Dynamics Drag Prediction Workshop, J. Aircr. 51(4) (2014) 1194–1213.

[19] X.-D. Liu, S. Osher, T. Chan, Weighted essentially non-oscillatory schemes, J. Comput. Phys. 115(1) (1994) 200–212.

[20] F. Shakib, T. Hughes, Z. Johan, "A new finite element formulation for computational
fluid dynamics: X. The compressible Euler and Navier-Stokes equations"
Computer Meth. in Appl. Mech. and Eng., Vol. 89, 1991, pp. 141-219.

[21] E. Tadmor, Entropy stability theory for difference approximations of nonlinear conservation laws and related time-dependent problems, Acta Numer. 12 (2003) 451–512.

[22] N.K. Yamaleev, M.H. Carpenter, A systematic methodology for constructing high-order energy stable WENO schemes, J. Comput. Phys. 228(11) (2009) 4248–4272.